THE JOURNAL OF PHYSICAL CHEMISTRY C

Article

pubs.acs.org/JPCC

Ligand-Mediated Electrocatalytic Activity of Pt Nanoparticles for Oxygen Reduction Reactions

Zhi-You Zhou,[†,‡] Xiongwu Kang,[†] Yang Song,[†] and Shaowei Chen*[,†]

[†]Department of Chemistry and Biochemistry, University of California, 1156 High Street, Santa Cruz, California 95064, United States

[‡]State Key Laboratory of Physical Chemistry of Solid Surfaces, Department of Chemistry, College of Chemistry and Chemical Engineering, Xiamen University, Xiamen 361005, China

Supporting Information

ABSTRACT: High-performance electrocatalysts for oxygen reduction reactions (ORR) are crucial for the development of proton exchange membrane fuel cells (PEMFCs). In this study, a novel method was developed by which the ORR activity of Pt nanoparticles was deliberately manipulated by selective organic capping ligands. By coreduction of diazonium salts and H_2PtCl_4, a series of Pt nanoparticles (core size 2.0−2.5 nm) stabilized by para-substituted (R = $-CH_3$, −F, −Cl, $-OCF_3$, and $-CF_3$) phenyl groups were synthesized. The experimental results demonstrated that the electron-withdrawing capability of the substituent moieties, as manifested by the Hammet substituent constant (σ), plays a key role in controlling the ORR activity, where the higher σ, the higher ORR activity. Within the present experimental context, Pt nanoparticles stabilized by trifluoromethylphenyl groups (Pt−Ar−CF_3) exhibit the highest catalytic activity among the series, with an ORR specific activity 3.2 times higher than that of commercial Pt/C catalysts. The enhanced activity may be correlated with the weakened oxygen adsorption by the electronegative ligands.

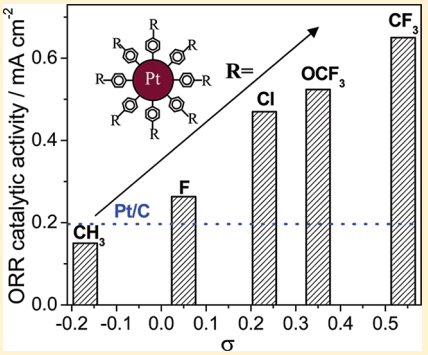

1. INTRODUCTION

Proton exchange membrane fuel cells (PEMFCs) are one promising clean and efficient power source for automobiles. The cathodic reaction of the PEMFCs is oxygen reduction reactions (ORR), i.e., $O_2 + 4H^+ + 4e^- \rightarrow 2H_2O$. Currently, poor performance of electrocatalysts for ORR is a major bottleneck for the commercialization of PEMFCs. The sluggish kinetics of ORR dictates that a high loading of expensive Pt catalysts has to be used in the cathodic catalyst layer of PEMFCs. In the past decades, a variety of strategies have been proposed and employed to improve the ORR activity of Pt nanoparticles that typically involve manipulation of the composition, size, and surface atomic arrangements of the nanoparticle catalysts. Of these, Pt-alloy catalysts (e.g., PtCo, PtNi, PtFe alloys) show significantly enhanced ORR activity as compared with pure Pt;[1−5] however, the preferential leaching of non-noble elements in the Pt-based alloys usually results in severe degradation of the nanoparticle catalysts and proton exchange membranes (the resulting metal ions will replace protons in the membranes).[6] In some other studies, polyhedral Pt nanocrystals (such as Pt nanocubes) have dominant surface sites with specific atomic arrangements that may possess high intrinsic activity.[7] Unfortunately, the particle sizes are usually too large (>5 nm) to be applied in practical fuel cells due to low Pt utilization (i.e., low surface-to-volume ratios). Additionally, the surfaces are usually covered by long-chain surfactants (such as polyvinylpyrrolidone (PVP), cetyltrimethylammonium bromide (CTAB), and oleylamine) that severely decrease the surface accessibility and catalytic activity,[8] so that some fairly tedious procedures have to be used to clean the Pt surfaces.

Recently, chemical functionalization of noble metal surfaces with specific molecules/ions to improve electrocatalytic performance has received increasing attention.[9−11] For example, the Markovic group has reported that the adsorption of CN^- on Pt(111) can greatly suppress the specific adsorption of SO_4^{2-} and PO_4^{3-} that blocks surface sites for ORR.[10] As a result, the ORR activity on the CN-modified Pt(111) shows a 25-fold increase in H_2SO_4 solution, and a 10-fold increase in H_3PO_4 solution, as compared with naked Pt(111) in the corresponding solutions. But the activities in $HClO_4$ solution are similar before and after CN^- modification. We have also shown that chlorophenyl-stabilized Pt nanoparticles (core diameter 1.85 nm) exhibit an ORR activity 2−3 times that of naked Pt nanoparticles in 0.1 M $HClO_4$.[12] This enhancement in ORR activity is much higher than that of triphenylphosphine triphosphonate (TPPTP) modification reported by Pietron et al.,[13] which only exhibited ∼22% improvement over Pt/C.

Herein, we carried out a systematic study to examine the effects of phenyl para-substituent groups on the ORR activity of aryl-stabilized Pt nanoparticles. It is well-known that in a polysubstituted benzene molecule there exist rather apparent electronic interactions between the substituent moieties. For example, the acidity of para-substituted benzoic acid increases

Received: January 6, 2012
Revised: April 25, 2012
Published: April 26, 2012

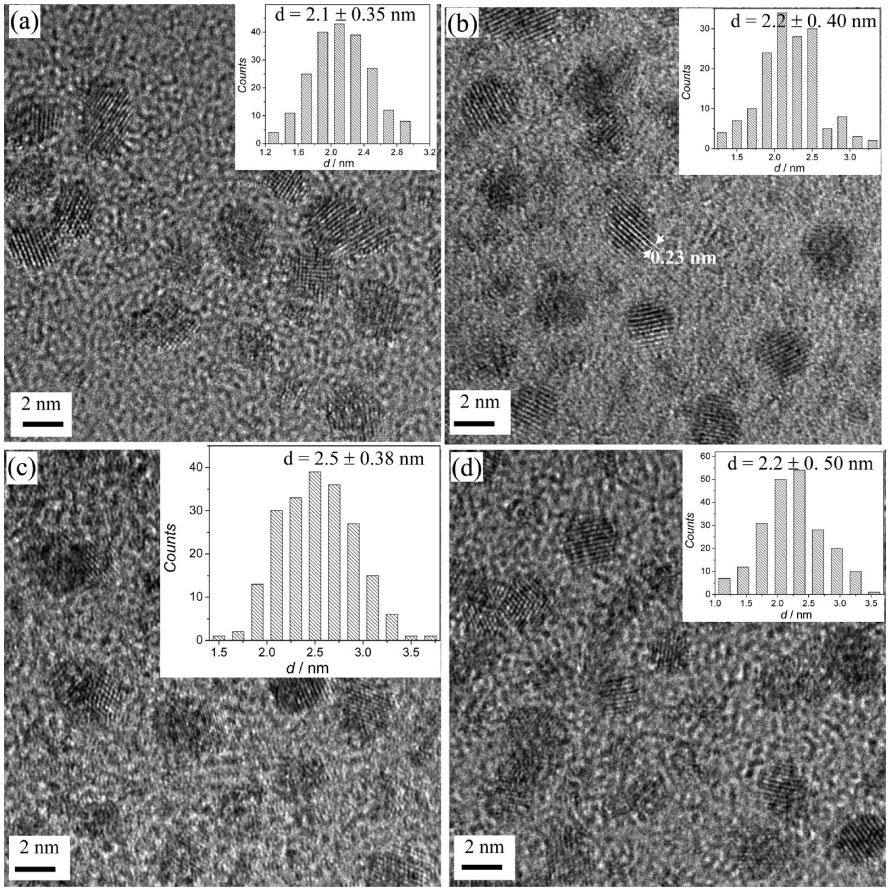

Figure 1. Representative HRTEM images of (a) Pt−Ar−CH_3, (b) Pt−Ar−F, (c) Pt−Ar−OCF_3, and (d) Pt−Ar−CF_3 nanoparticles. White lines in (b) highlight the lattice fringes with a spacing of 0.23 nm, corresponding to the (111) lattice of Pt. Insets are the corresponding core size histograms.

with increasing electronegativity of the para substituents.[14] Experimentally, we prepared a series of Pt nanoparticles with similar particle sizes but capped with different substituent aryl groups grafted through the formation of Pt−C covalent bonds. The results indicate that the ORR activity of the resulting Pt nanoparticles increases with the substituents in the order of $-CH_3 < -F < -Cl < -OCF_3 < -CF_3$, which is in line with the increase of their electron-withdrawing capability, according to the corresponding Hammet substituent constants (σ).[14,15] The enhanced ORR activity may be rationalized by the weakening of oxygen adsorption on Pt.

2. EXPERIMENTAL SECTION

2.1. Chemicals. Platinum chloride ($PtCl_2$, 73% Pt, ACROS), *p*-toluidine (i.e., 4-methylaniline, 99%, ACROS), 4-fluoroaniline (99%, Alfa Aesar), 4-chloroaniline (98%, ACROS), 4-(trifluoromethoxy)aniline (98%, Alfa Aesar), 4-(trifluoromethyl)aniline (97%, Maybridge), sodium borohydride ($NaBH_4$, 98%, ACROS), sodium nitrite ($NaNO_2$, 98%, ACROS), perchloric acid ($HClO_4$, 70 wt %, ACROS), toluene (HPLC grade, Fisher Scientific), tetrahydrofuran (THF, HPLC grade, Fisher Scientific), and high-purity O_2 (99.993%, Praxair Inc.) were used as received. A commercial Pt/C catalyst was purchased from Alfa Aesar (20 wt %, HiSPEC3000, Johnson Matthey). Water was supplied by a Barnstead Nanopure water system (18.3 MΩ·cm).

2.2. Synthesis of Aryl-Stabilized Pt Nanoparticles. The nanoparticles were prepared by the coreduction of H_2PtCl_4 and aryl diazonium salts, a procedure that has been used previously for the synthesis of butylphenyl-stabilized Pd and Pt nanoparticles.[11,16] Briefly, the diazonium salts were synthesized from para-substituted anilines (0.5 mmol), sodium nitrite (0.52 mmol), and 35% perchloric acid (0.45 mL) in an ice−water bath. Five para-substituted (R) anilines were used in this study, with R = $-CH_3$, −F, −Cl, $-OCF_3$, and $-CF_3$. The resulting diazonium salt and H_2PtCl_4 (0.1 mmol) were codissolved in a mixed solvent of H_2O−THF (1:1, v/v), into which a freshly prepared $NaBH_4$ solution (0.2 M, 5 mL) was added slowly under magnetic stirring, leading to the formation of a dark brown solution that signified the production of aryl-stabilized Pt nanoparticles.[17,18]

The raw products were extracted by toluene and washed by 0.1 M H_2SO_4 solution and Nanopure water several times. After most of the solvent was rotary evaporated, the Pt nanoparticles were precipitated by a specific solvent depending on the polarity of the aryl ligands. For nonpolar $-CH_3$ group, ethanol was used as the precipitant, and Pt nanoparticles were collected by centrifugation and further washed four times with ethanol to remove impurities and excessive free ligands. Finally, the purified Pt nanoparticles were dissolved in THF. The Pt nanoparticles with other polar substituents were precipitated by hexane and further washed with hexane−ethanol (5:1). The purified Pt nanoparticles were dissolved in ethanol. The resulting Pt nanoparticles were denoted as Pt−Ar−R with R = CH_3, F, Cl, OCF_3, and CF_3.

2.3. Structural Characterizations. The morphology and sizes of the Pt−Ar−R nanoparticles were characterized by transmission electron microscopy studies (TEM, Philips

dx.doi.org/10.1021/jp300199x | J. Phys. Chem. C 2012, 116, 10592−10598

CM300 at 300 kV). More than 200 nanoparticles were measured to obtain a size histogram. FTIR spectroscopic measurements (Perkin-Elmer Spectrum One FTIR spectrometer) were carried out to characterize the surface ligands on the nanoparticle surface. The samples were prepared by dropcasting a concentrated solution of the nanoparticles onto a ZnSe disk. After solvent evaporation, a uniform film of nanoparticles was formed. Surface-enhanced Raman spectroscopic (SERS) measurements were carried out with a Nicolet Almega XR dispersive Raman spectrometer (laser wavelength 780 nm). The procedure of substrate preparation was included in the Supporting Information. The amount of organic ligands on the Pt nanoparticles was determined by thermogravimetric analysis (TGA, Perkin-Elmer Pyris 1 thermogravimetric analyzer) under a high-pure N_2 (99.999%) flow at a temperature rate of 10 °C min^{-1}.

2.4. Electrochemistry. Electrochemical studies were carried out in a standard three-electrode cell connected to a CHI-440 electrochemical workstation, with a Pt foil counter electrode and a reversible hydrogen electrode (RHE) at room temperature (~20 °C). Working electrode is a rotating disk electrode (RDE, glassy carbon (GC), ϕ = 5 mm) purchased from Pine Instrument, Inc.

To prepare catalyst solutions for ORR tests, dilute solutions of the aryl-stabilized Pt nanoparticles in ethanol were mixed with XC-72 carbon black and a Nafion 117 solution (5 wt %, Fluka) to form a well dispersed catalyst "ink" (Pt:carbon black = 1:4 (w/w), 0.20 mg_{Pt} mL^{-1}, Nafion: 0.05%) under ultrasound. For Pt−Ar−CH_3 nanoparticles, the procedure was slightly different where a mixed solvent of THF−ethanol (1:1) was used instead in order to obtain a uniform dispersion. Similarly, the commercial Pt/C (20 wt %, Johnson Matthey) was also dispersed in ethanol containing Nafion (0.05%) to form a catalyst ink (0.20 mg_{Pt} mL^{-1}) under ultrasound.

To prepare the working electrode, a calculated amount of the catalyst inks was slowly drop-cast onto a polished glassy carbon (GC, ϕ = 5 mm) rotating disk electrode. To obtain a uniform catalyst layer, the GC electrode was slowly rotated at a rate of 300 rpm during the drying process. As soon as the electrode was dried, a dilute Nafion solution (0.1 wt %, 3 μL) was added onto it. The Pt loading on the GC electrode was 2.0−2.5 μg.

Prior to the ORR tests, the Pt nanoparticle films on the GC electrode were electrochemically pretreated in N_2-saturated 0.1 M $HClO_4$ through potential cycling at 0.1 V s^{-1} between +0.05 and +1.3 V for 5−10 cycles. The electrocatalytic activity for ORR was then evaluated in an O_2-saturated 0.1 M $HClO_4$ solution by using a rotating (ring) disk electrode system (Pine Instrument Inc.) at a rotation rate of 1600 rpm. Electrode potential was scanned from +0.05 to +1.3 V at 10 mV s^{-1}, and the solution ohmic drop (i.e., *IR* drop) was electronically compensated. The steady forward polarization curves were used to calculate the ORR activity.

3. RESULTS AND DISCUSSION

3.1. TEM Characterization. Figure 1 shows representative HRTEM images of the as-prepared Pt nanoparticles stabilized by −CH_3, −F, −OCF_3, and −CF_3 substituted phenyl groups. The HRTEM image of chlorophenyl-stabilized Pt nanoparticles with an average core size of 1.85 nm has been reported previously.[12] In Figure 1, well-defined lattice fringes, with a spacing of 0.23 nm corresponding to the (111) lattice spacing of Pt, can be clearly observed for all samples. The average core sizes of the Pt nanoparticles are similar, in the range of 2.1−2.5 nm, with a rather narrow dispersity (<20%). These particle sizes are smaller than the typical dimensions (~3.3 nm) of commercial Pt/C catalysts used as a comparative sample in this study (Figure S1).

3.2. FTIR Characterization. Figure 2 shows the transmission infrared spectra of the above aryl-stabilized Pt

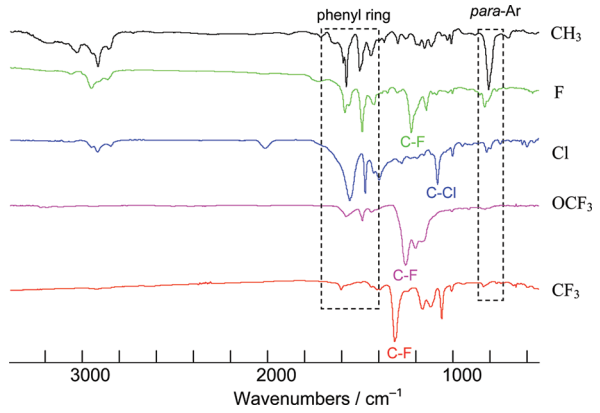

Figure 2. Transmission IR spectra of aryl-stabilized Pt nanoparticles.

nanoparticles. The IR characteristic peaks of the phenyl rings can be identified in two regions (dashed boxes). One region is between 1460 and 1620 cm^{-1}, where two or three bands can be observed, corresponding to the C=C skeleton stretches in the phenyl ring. In comparison with free ligands (e.g., the corresponding aniline and substituted benzene), the aromatic ring skeleton vibration peaks shift to lower wavenumbers, and the peak width becomes slightly broader.[11,12] These results suggest that there are relatively strong electronic interactions between the aromatic rings and metal nanoparticles. The other region is near 850 cm^{-1}, which corresponds to the out-of-plane C−H deformation vibration in para-substituted phenyl rings. In addition, there exist characteristic peaks for the specific substituent groups, such as the stretch vibration of C−F (1233 cm^{-1} for Pt−Ar−F; 1264 cm^{-1} for Pt−Ar−OCF_3; and 1322 cm^{-1} for Pt−Ar−CF_3) and C−Cl (1092 cm^{-1} for Pt−Ar−Cl). These IR characteristics confirm that the Pt nanoparticles were indeed functionalized by the respective aryl ligands.

It is worth noting that the vibrational feature of the Pt−C bonds, located at very low wavenumbers (in the far-infrared region), is hardly detected by conventional IR spectroscopic measurements. Theoretical calculations have shown that phenyl (C_6H_5) groups can be attached onto Cu, Au, and Pd surfaces through M−C covalent bonds, and Pd exhibits the highest binding energy.[19] For aryl-capped Au nanoparticles (core size 40 nm), Laurentius et al.[20] provided direct evidence for the formation of Au−C covalent bonds by using surface-enhanced Raman scattering (SERS) measurements. However, the SERS effect of Pt nanoparticles of 2−3 nm in diameter is too weak to be detected. Yet it is well documented that electrochemical reduction of diazonium salts is an alternative approach to the formation of aryl-grafted metal surfaces.[18,21] Thus, to detect Pt−C by SERS measurements, we prepared a SERS-active Pt substrate where two monolayers of Pt were deposited onto an electrochemically roughened Au electrode (Pt(2 ML)/Au), by adopting a procedure used by the Weaver group (details in the Supporting Information).[22] The aryl groups were then grafted on the Pt(2 ML)/Au surface through electrochemical reduction of the corresponding diazonium salts. SERS measurements

dx.doi.org/10.1021/jp300199x | J. Phys. Chem. C 2012, 116, 10592−10598

show a well-defined band at 410−420 cm^{-1} for all samples (Figure 3). Previously, Koper et al. have reported that Pt−CH_x

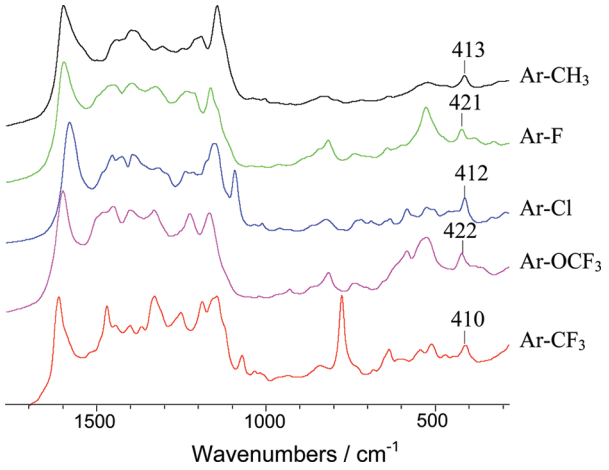

Figure 3. SERS spectra of varied aryl fragments grafted onto the Pt(2 ML)/Au substrate.

exhibited a SERS peak at around 420 cm^{-1} which was assigned to the Pt−C bond.[23] Therefore, the band between 410 and 420 cm^{-1} observed in the present study may be attributed to the Pt−C bond on the aryl-capped Pt surface, further confirming the covalent grafting of the aryl ligands onto the Pt nanoparticle surface.

3.3. Thermogravimetric Analysis. Thermogravimetric analysis (TGA) was then employed to quantitatively evaluate the amount of organic ligands on the Pt nanoparticle surface. As shown in Figure 4, the weight loss of all the nanoparticle

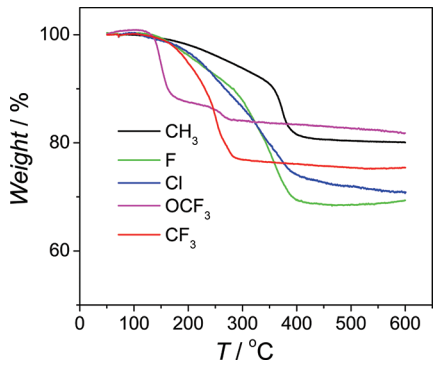

Figure 4. TGA curves of Pt−Ar−R nanoparticles measured under a N_2 atmosphere at a heating rate of 10 °C min^{-1}. The R substituent groups are specified in the figure legends.

samples started to occur at ∼150 °C and peaked around 300 °C, with a total weight loss ranging from 16% to 32% (Table 1). On the basis of the weight loss and the average core size of the Pt nanoparticles determined by TEM measurements (Figure 1), the average area occupied by one ligand on the Pt nanoparticle surface was estimated to range from 4.5 to 15.7 $Å^2$ (Table 1). Note that in a previous study Mirkhalaf et al.[17] reported the synthesis of decylphenyl-stabilized Pt nanoparticles, where the cross-sectional area per ligand was determined to be about 5.5 $Å^2$. These values are somewhat lower than the typical value (∼20 $Å^2$) for long-chain alkanethiolates adsorbed on metal nanoparticles.[24] On a Pt nanoparticle, the area per Pt atom is 6.65 $Å^2$ on the {111} facet

Table 1. Physical Parameters of Pt−Ar−R Nanoparticles and Their Electrocatalytic Activity for ORR

substituent (R)	CH_3	F	Cl[a]	OCF_3	CF_3	Pt/C
σ^b	−0.017	+0.05	+0.23	+0.35	+0.54	
particle size (nm)	2.1	2.1	1.85	2.5	2.2	3.3
weight loss (%)	20	32	26	16	19	
area per ligand ($Å^2$)	8.0	4.5	8.0	15.7	13.0	
specific ECSA ($m^2\ g^{-1}_{Pt}$)	54	54	93	47	59	80
j_k (mA cm^{-2} at +0.90 V)	0.15	0.30	0.47	0.52	0.65	0.20
j_m (mA mg^{-1}_{Pt} at +0.90 V)	0.082	0.162	0.437	0.244	0.384	0.16

[a]Data from ref 12. [b]Hammet substituent constant (σ) from ref 15.

and 7.68 $Å^2$ on the {100} facet. The low occupying area by the aryl groups, as observed in the present study and others,[17] suggests that the ligands may form a multilayer (e.g., oligoaryl) structure on the Pt nanoparticles.[25]

3.4. Ligand-Mediated ORR Electrocatalyst Activity. Figure 5a shows the forward-scan ORR polarization curves of

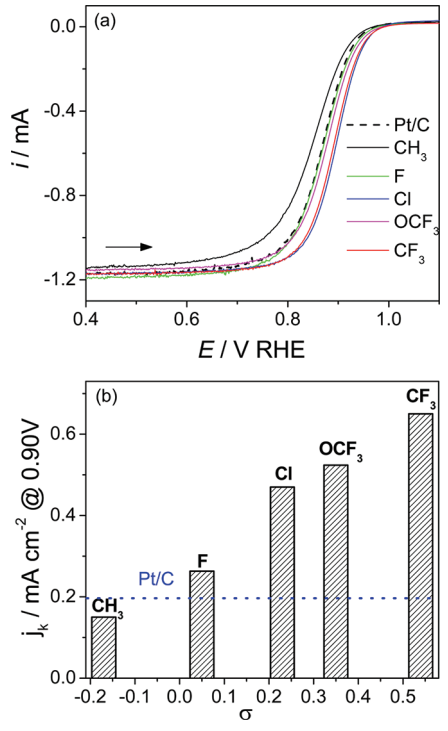

Figure 5. (a) Forward-scan ORR polarization curves of the Pt−Ar−R nanoparticles and commercial Pt/C catalyst in an O_2-saturated 0.1 M $HClO_4$ solution at room temperature. Electrode rotating rate: 1600 rpm; potential scan rate: 10 mV s^{-1}. Pt loading: CH_3 (2.5 μg), F (2.4 μg), and all others 2.0 μg of Pt. (b) Variation of the ORR specific activity (j_k at +0.90 V) with Hammet substituent constant (σ). Blue dotted line denotes the ORR activity of commercial Pt/C catalysts.

the Pt−Ar−R nanoparticles in an O_2-saturated 0.1 M $HClO_4$ solution. The dotted line is the curve for commercial Pt/C. Clearly, methylphenyl-stabilized Pt nanoparticles exhibit the lowest catalytic activity among the series. To quantitatively compare the intrinsic catalytic activity, the specific activity was calculated by the Koutecky−Levich equation (eq 1) where the

dx.doi.org/10.1021/jp300199x | J. Phys. Chem. C 2012, 116, 10592−10598

kinetic current (i_k) was separated from the mass transfer component

$$\frac{1}{i} = \frac{1}{i_L} + \frac{1}{i_k} \quad (1)$$

In eq 1, i and i_L are the observed current measured at a specific electrode potential (e.g., +0.90 V) and diffusion limiting current (i.e., current plateau at E < +0.60 V), respectively. The ORR intrinsic catalytic activity, defined by the area-specific activity or kinetic current density (j_k), was obtained by normalizing i_k to the (effective) electrochemical surface area (ECSA) of Pt. The latter was determined by the charge of hydrogen adsorption and desorption on Pt between +0.05 and +0.40 V, on the assumption of a charge density of 0.21 mC cm^{-2} (Figure 6a and

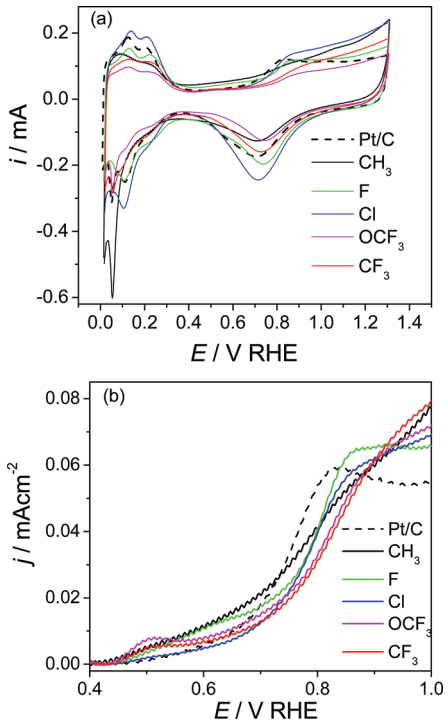

Figure 6. (a) Cyclic voltammograms of aryl-stabilized Pt nanoparticles and commercial Pt/C catalyst in N_2-saturated 0.1 M HClO4 at 100 mV s^{-1}. The samples are the same as those used in ORR tests in Figure 5. (b) Enlarged cyclic voltammograms near oxygen-adsorption region in the forward-going scan. The current has been normalized to the ECSA, and double-layer charging current has also been corrected.

Table 1). To gain insights into the electronic effects of the substituent groups on the ORR activity, the j_k at +0.90 V was plotted as a function of the Hammet substituent constant (σ), as shown in Figure 5b. The Hammet substituent constant (σ) is an empirical parameter that quantitatively describes the electron-withdrawing capability of substituent groups on a phenyl ring, where both inductive effect and resonance effect are taken into account.[14,15] The more positive σ, the higher electron-withdrawing capability of the substituent. Note that the F substituent group has a σ value less than that of Cl because of a much larger resonance effect (electron donation) than that of the latter.

In Figure 5b, one can see that the j_k value increases with increasing σ; that is, electron-withdrawing substituents are favorable to the electrocatalytic activity for ORR (Table 1), in the order of Pt−Ar−CH_3 < Pt/C < Pt−Ar−F < Pt−Ar−Cl < Pt−Ar−OCF_3 < Pt−Ar−CF_3. Of these, the j_k value of Pt−Ar−CF_3, the most active catalyst among the series, is as high as 0.65 mA cm^{-2}, more than 3 times that of commercial Pt/C (0.20 mA cm^{-2}) and 4 times that of Pt−Ar−CH_3 (0.15 mA cm^{-2}). It is worth noting that the fractions of electrochemically accessible surface sites, which are related to the surface coverage of organic ligands, are quite close for all of the aryl-stabilized nanoparticle samples, varying from 0.41 to 0.62. Thus, it is unlikely that the enhanced catalytic activity as manifested in Figure 5 arises from the different coverage of ligands alone (Figure S2). Furthermore, if the kinetic current is normalized to the overall surface area estimated from the average core size of Pt nanoparticles, the activities of Pt−Ar−Cl (0.29 mA cm^{-2}) and Pt−Ar−CF_3 (0.30 mA cm^{-2}) remain significantly larger than that of Pt/C. Actually, when the negative size effect on the ORR activity of Pt nanoparticles is taken into account,[26−28] the enhancement of the nanoparticle ORR activity by aryl surface functionalization is much more profound. This enhancement (over 200% for Pt−Ar−CF_3 over Pt/C) is also greatly higher than that of Pt nanoparticles stabilized by TPPTP (~22% improvement in specific activity)[13] and thiol.[29,30]

For practical applications, the ORR current provided by per gram of Pt is an important criterion. This can be evaluated by the mass activity (j_m); i.e., the kinetic current normalized by the mass of Pt loaded on the electrodes. As shown in Table 1, the order of j_m was somewhat different from j_k, Pt−Ar−CH_3 < Pt/C < Pt−Ar−F < Pt−Ar−OCF_3 < Pt−Ar−CF_3 < Pt−Ar−Cl, where Pt−Ar−Cl shows the highest value of 0.437 mA mg$^{-1}_{Pt}$ at +0.90 V, largely because it has a very high specific ECSA (96 m^2 g$^{-1}_{Pt}$).[12] The Pt−Ar−CF_3 nanoparticles (0.384 mA mg$^{-1}_{Pt}$) also show a mass activity 2.4 times higher than that of Pt/C (0.16 mA mg$^{-1}_{Pt}$). In additions, we found previously that surface functionalization of commercial Pt/C with ArCl doubled the ORR mass activity, although the ECSA decreased by about 30%.[12] These results strongly suggest that surface functionalization of Pt nanoparticles with selective aryl groups is indeed a promising and unique approach to the further improvement of the ORR activity.

Similar to Pt-based alloys,[2] the enhanced catalytic activity of the Pt−Ar−R nanoparticles, as compared with "naked" commercial Pt/C catalysts, may be correlated with the weakened adsorption of oxygen species (e.g., O_{ad} and OH_{ad}) on the Pt surfaces. It has been demonstrated that the reductive desorption of adsorbed oxygen species to form water is the sluggish step during ORR on Pt surface, so that the deceasing oxygen binding energy will favor the ORR catalytic activity.[2,31] Figure 6a shows the cyclic voltammograms (CVs) recorded in N_2-satuarted 0.1 M $HClO_4$ for the Pt−Ar−R nanoparticles right after the ORR tests. To compare the adsorption of oxygen species, Figure 6b shows the voltammetric curves around the onset of oxygen adsorption. The current has been normalized to the corresponding ECSA, and the double-layer charging current has been corrected. It can be clearly seen that the voltammetric current of oxygen adsorption in the range of +0.70 to +0.90 V increases in the order of Pt/C > Pt−Ar−F > Pt−Ar−Cl > Pt−Ar−OCF_3 > Pt−Ar−CF_3, which is in the reverse order of ORR activity as manifested in Figure 5 (and Table 1). Note that the current of oxygen adsorption on Pt−Ar−CH_3 is moderate in this potential region, but the current near +0.70 V is much higher than those of other samples, indicating that oxygen adsorption occurs more easily on Pt−Ar−CH_3 at low potentials. Overall, it can be concluded that the enhanced ORR activity was most likely due to the weakening of

dx.doi.org/10.1021/jp300199x | J. Phys. Chem. C 2012, 116, 10592−10598

oxygen adsorption on the Pt nanoparticle surface. In other words, the above experimental observations suggest that aryl functionalization may have changed the electronic structure of the Pt nanoparticles and hence oxygen adsorption.

For oxygen adsorption on Pt, electron is transferred from Pt to oxygen.[32] When the surface is coadsorbed with substituted aryl groups, the electron density of Pt and thus oxygen adsorption may be varied by the electronegativity of the substituent moieties (Figure 7). Specifically, electron-withdrawing substituents (e.g., F, Cl, OCF_3, and CF_3) will likely decrease the electron density of Pt surface atoms, which is unfavorable for the adsorption of oxygen atoms. To gain in-depth knowledge of this ligand effect on the ORR activity, further studies based on theoretical calculations are desired, by which the electronic structures of aryl-stabilized Pt nanoparticles may be elucidated clearly. It is also worth noting that there is a hump at about +0.50 V in the voltammetric measurements (Figure 6), which appears to be electrochemically (quasi)reversible (Figure S3). The origin of this is not clear at the moment, and further studies are needed.

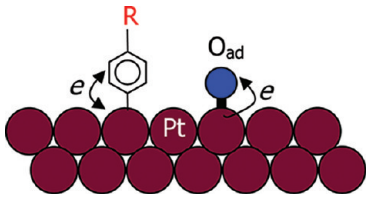

Figure 7. Schematic illustration of the impact of aryl capping groups on oxygen adsorption. Electronegative ligands will compete with oxygen atoms to withdraw electron from Pt, leading to weakened oxygen adsorption.

The yield of H_2O_2 during ORR on the aryl-stabilized Pt nanoparticles is also very low, e.g., only 1.3% on the Pt−Ar−Cl nanoparticles[12] and 1.3% on Pt−Ar−CF_3 (Figure S4), which are very close to that of naked Pt (~1%).[33] As for electrochemical stability, previous result indicated that Pt−Ar−Cl nanoparticles and Pt/C suffered similar loss in the ECSA during continuously potential cycling between +0.05 and +1.30 V, but the ORR activity of Pt−Ar−Cl nanoparticles remained markedly higher than that of Pt/C.[12]

4. CONCLUSIONS

In summary, a series of aryl-stabilized Pt nanoparticles (core size 2.0−2.5 nm) have been synthesized through the coreduction of aryl diazonium salts and Pt precursors. The para substituents on the phenyl ring were deliberately varied from CH_3 to F, Cl, OCF_3, and CF_3 that exhibited increasing electron-withdrawing capability, as reflected by their Hammet constants (σ). Transmission IR measurements of these aryl-stabilized Pt nanoparticles showed the corresponding vibrational characteristics of the substituent moieties. Thermogravimetric analysis indicated that the organic components accounted for 16% to 40% of the nanoparticle mass, suggesting the existence of an oligoaryl structure (i.e., multilayers of ligands) on the nanoparticle surface. Electrocatalytic studies demonstrated that the phenyl substituents greatly influenced the ORR activity of the Pt nanoparticles. Specifically, the area-specific activity of ORR increased with increasing electron withdrawing capability of the substituents. Of these, trifluoromethylphenyl-stabilized Pt nanoparticles (Pt−Ar−CF_3) were the most active catalyst, with an area-specific activity 3.2 times higher than that of commercial Pt/C catalyst. The enhanced ORR electrocatalytic activity may be correlated with the weakened oxygen adsorption by the electronegative ligands. The present study demonstrates that surface functionalization of noble metal nanoparticles by selective organic ligands may be a unique and promising approach to improving electrocatalytic activity in fuel cell electrochemistry.

■ ASSOCIATED CONTENT

Supporting Information

Complete list of ref 24, TEM images of Pt/C, SERS substrate preparation, and additional CV curves. This material is available free of charge via the Internet at http://pubs.acs.org.

■ AUTHOR INFORMATION

Corresponding Author

*E-mail: shaowei@ucsc.edu.

Notes

The authors declare no competing financial interest.

■ ACKNOWLEDGMENTS

This work was supported by the National Science Foundation (CHE-1012258) and the ACS-Petroleum Research Fund (49137-ND10). TEM studies were carried out at the National Center for Electron Microscopy, Lawrence Berkeley National Laboratory, which is supported by the Department of Energy.

■ REFERENCES

(1) Paulus, U. A.; Wokaun, A.; Scherer, G. G.; Schmidt, T. J.; Stamenkovic, V.; Radmilovic, V.; Markovic, N. M.; Ross, P. N. *J. Phys. Chem. B* **2002**, *106*, 4181−4191.
(2) Stamenkovic, V. R.; Fowler, B.; Mun, B. S.; Wang, G. F.; Ross, P. N.; Lucas, C. A.; Markovic, N. M. *Science* **2007**, *315*, 493−497.
(3) Toda, T.; Igarashi, H.; Uchida, H.; Watanabe, M. *J. Electrochem. Soc.* **1999**, *146*, 3750−3756.
(4) Peng, Z. M.; Yang, H. *J. Am. Chem. Soc.* **2009**, *131*, 7542−7543.
(5) Koh, S.; Strasser, P. *J. Am. Chem. Soc.* **2007**, *129*, 12624−12625.
(6) Xu, Q. M.; Kreidler, E.; He, T. *Electrochim. Acta* **2010**, *55*, 7551−7557.
(7) Wang, C.; Daimon, H.; Lee, Y.; Kim, J.; Sun, S. *J. Am. Chem. Soc.* **2007**, *129*, 6974−6975.
(8) Lee, H.; Habas, S. E.; Kweskin, S.; Butcher, D.; Somorjai, G. A.; Yang, P. D. *Angew. Chem., Int. Ed.* **2006**, *45*, 7824−7828.
(9) Genorio, B.; Strmcnik, D.; Subbaraman, R.; Tripkovic, D.; Karapetrov, G.; Stamenkovic, V. R.; Pejovnik, S.; Markovic, N. M. *Nat. Mater.* **2010**, *9*, 998−1003.
(10) Strmcnik, D.; Escudero-Escribano, M.; Kodama, K.; Stamenkovic, V. R.; Cuesta, A.; Markovic, N. M. *Nat. Chem* **2010**, *2*, 880−885.
(11) Zhou, Z. Y.; Kang, X. W.; Song, Y.; Chen, S. W. *Chem. Commun.* **2011**, *47*, 6075−6077.
(12) Zhou, Z. Y.; Kang, X. W.; Song, Y.; Chen, S. W. *Chem. Commun.* **2012**, *48*, 3391−3393.
(13) Pietron, J. J.; Garsany, Y.; Baturina, O.; Swider-Lyons, K. E.; Stroud, R. M.; Ramaker, D. E.; Schull, T. L. *Electrochem. Solid State Lett.* **2008**, *11*, B161−B165.
(14) Hammett, L. P. *J. Am. Chem. Soc.* **1937**, *59*, 96−103.
(15) Hansch, C.; Leo, A.; Taft, R. W. *Chem. Rev.* **1991**, *91*, 165−195.
(16) Zhou, Z. Y.; Ren, J.; Kang, X. W.; Song, Y.; Sun, S. G.; Chen, S. W. *Phys. Chem. Chem. Phys.* **2012**, *14*, 1412−1417.
(17) Mirkhalaf, F.; Paprotny, J.; Schiffrin, D. J. *J. Am. Chem. Soc.* **2006**, *128*, 7400−7401.
(18) Delamar, M.; Hitmi, R.; Pinson, J.; Saveant, J. M. *J. Am. Chem. Soc.* **1992**, *114*, 5883−5884.
(19) Jiang, D. E.; Sumpter, B. G.; Dai, S. *J. Am. Chem. Soc.* **2006**, *128*, 6030−6031.

(20) Laurentius, L.; Stoyanov, S. R.; Gusarov, S.; Kovalenko, A.; Du, R. B.; Lopinski, G. P.; McDermott, M. T. *ACS Nano* **2011**, *5*, 4219−4227.
(21) Belanger, D.; Pinson, J. *Chem. Soc. Rev.* **2011**, *40*, 3995−4048.
(22) Mrozek, M. F.; Xie, Y.; Weaver, M. J. *Anal. Chem.* **2001**, *73*, 5953−5960.
(23) Lai, S. C. S.; Kleyn, S. E. F.; Rosca, V.; Koper, M. T. M. *J. Phys. Chem. C* **2008**, *112*, 19080−19087.
(24) Hostetler, M. J.; Wingate, J. E.; Zhong, C. J.; Harris, J. E.; Vachet, R. W.; Clark, M. R.; Londono, J. D.; Green, S. J.; Stokes, J. J.; Wignall, G. D.; et al. *Langmuir* **1998**, *14*, 17−30.
(25) Adenier, A.; Combellas, C.; Kanoufi, F.; Pinson, J.; Podvorica, F. I. *Chem. Mater.* **2006**, *18*, 2021−2029.
(26) Shao, M. H.; Peles, A.; Shoemaker, K. *Nano Lett.* **2011**, *11*, 3714−3719.
(27) Mayrhofer, K. J. J.; Blizanac, B. B.; Arenz, M.; Stamenkovic, V. R.; Ross, P. N.; Markovic, N. M. *J. Phys. Chem. B* **2005**, *109*, 14433−14440.
(28) Kinoshita, K. *J. Electrochem. Soc.* **1990**, *137*, 845−848.
(29) Baret, B.; Aubert, P. H.; Mayne-L'Hermite, M.; Pinault, M.; Reynaud, C.; Etcheberry, A.; Perez, H. *Electrochim. Acta* **2009**, *54*, 5421−5430.
(30) Cavaliere, S.; Raynal, F.; Etcheberry, A.; Herlem, M.; Perez, H. *Electrochem. Solid State Lett.* **2004**, *7*, A358−A360.
(31) Greeley, J.; Stephens, I. E. L.; Bondarenko, A. S.; Johansson, T. P.; Hansen, H. A.; Jaramillo, T. F.; Rossmeisl, J.; Chorkendorff, I.; Norskov, J. K. *Nat. Chem.* **2009**, *1*, 552−556.
(32) Pang, Q.; Zhang, Y.; Zhang, J. M.; Xu, K. W. *Appl. Surf. Sci.* **2011**, *257*, 3047−3054.
(33) Yano, H.; Higuchi, E.; Uchida, H.; Watanabe, M. *J. Phys. Chem. B* **2006**, *110*, 16544−16549.